Nonequilibrium argon plasma generated by an electron beam

A. V. Vasenkov
Novosibirsk State University, Novosibirsk 630090, Russia
(Received 8 May 1997; revised manuscript received 15 September 1997)

Energy- and space-dependent electron flux has been computed by a Monte Carlo method for 0.1–10.0 keV incident electrons in argon. This flux can be employed to calculate the efficiency for production of any electron state at any spatial position along the beam axis. Because of the simple characteristics of electron flux, its analytical approximation is represented. The formula for the path length of the complete electron energy degradation (range) versus incident energy for various gaseous media was obtained and compared successfully with the range data available from the current literature. [S1063-651X(98)03101-8]

PACS number(s): 52.20.Fs, 52.40.Mj, 52.65.−y, 34.80.Gs

I. INTRODUCTION

The energy- and space-dependent electron flux contains the basic information about the radiation field of electrons in an electron-beam-generated plasma. The requirement to compute electron flux occurs in aeronomy, radiation dosimetry, experimental diagnostics, and electron-beam technology. The energy-depositional aspects of interaction of energetic particles with gases, important for investigation of auroral phenomena, has a long literature list [1,2]. Less attention was given to the study of properties of electron-beam-generated plasmas used in electron-beam technologies, particularly in methods used to deposit thin films with ionized gas flows [3–6]. Since the degree of ionization in these plasmas is small ($\leqslant 10^{-6}$), the influence of Coulomb collisions on the electron flux density is negligible [7]. The purpose of this paper is to obtain (for energy above the first excitation potential of argon) the energy- and space-dependent electron flux in an electron-beam-generated plasma of Ar. The currently available data on the electron energy distribution being formed, when the incident electron and all its secondaries and tertiaries degrade completely in energy, have been obtained by Elliot and Greene [8], Green *et al.* [9], Keto [10], Kowari *et al.* [11], Kimura *et al.* [12]. Many detailed studies concerning the electron energy distribution have been reviewed recently by Kimura *et al.* [13]. However, to our knowledge, no work exists on the study of the energy- and space-dependent distribution of electrons generated by a nonrelativistic electron beam. Our choice of a set of cross sections for Ar is presented in Sec. II. Then a brief review of the techniques used for the modeling an electron-beam-generated plasma is given in Sec. III. Our results on the electron energy degradation process are compared with previous calculations of various authors in Sec. IV. The energy- and space-dependent electron flux is used for calculation of the efficiency for production of any electron state at any spatial position along the beam axis in Sec. V. Because of the simple characteristics of electron flux, its analytical approximation is represented in this section. The range versus energy relation for molecular hydrogen, atomic oxygen, molecular nitrogen, and argon is discussed in Sec. VI.

II. CROSS SECTIONS

In this section we present the set of cross sections that we have assembled and used for simulation of electron-beam-generated plasma of argon. To describe the available differential elastic scattering determinations for electrons in Ar, we developed analytical fits to these data, which are useful for Monte Carlo calculations. For this purpose, the most convenient method of tabulating the differential scattering data is the analysis of various experimental and theoretical determinations in terms of phenomenological extension of the screened Rutherford formula as defined in Eq. (4). This formula includes forward, medium-angle, and backward scattering components. The results of fitting are summarized in Table I. The study by Chutjian and Cartwright [14] presents inelastic differential cross sections for several excitation states of Ar at electron energies between 16 and 100 eV. These data show that for 16–100 eV electrons, collisions with excitation of optically allowed states cause approximately the same amount of scattering as that resulting from elastic collisions, while differential scattering cross sections for collisions with excitation of optically forbidden states may be approximately represented by isotropic scattering function. For energy above 100 eV for the current computations we have assumed that the angular deflection on inelastic scattering is negligible. Doubly differential ionization cross sections published by DuBois and Rudd [15] imply that the angular distribution for the secondary electron produced in Ar is similar that in N_2. Test comparisons for an electron-beam-generated plasma of nitrogen made by Jackman and Green [16] revealed that changing the secondary doubly differential ionization cross section to an isotropic secondary scattering function does not affect the electron distribution in energies and space. Therefore, in this work secondary electrons are assumed to be produced with an isotropic angular distribution. Because of the importance of inelastic collisions, we have examined the total inelastic cross-section data available in the literature more thoroughly than previously [17]. We have considered experimental and theoretical determinations of cross sections of inelastically scattered electrons and have represented these data as a function of the type presented by Porter *et al.* [18].

In general, our approach in deriving this set of cross sections for energy above the first excitation potential of argon

TABLE I. Parameters used in Eq. (4).

E	$10^{+3}\ \gamma$	μ	h_1	h_2	h_3	d_1	d_2	d_3	B_1	B_2	s	θ'
10	191	0.0946	0.746	0.969	0.703	8.1	80.2	27.3	0.945	0.313	2.361	−1.364
20	151	0.112	0.600	0.936	0.563	24.1	121.7	13.6	0.503	0.116	0.407	−1.760
30	129	0.105	0.595	0.941	0.913	46.7	90.9	27.6	0.988	0.0720	0.621	−1.864
40	68.7	0.0705	0.618	0.917	0.871	48.7	117.9	110.5	2.34	0.0509	0.669	−1.812
50	43.8	0.0642	0.586	0.964	0.825	72.0	79.5	74.1	5.48	0.117	1.309	−1.792
60	28.6	0.0700	0.615	0.956	0.737	55.1	67.1	56.7	8.49	0.343	1.595	−1.716
80	22.3	0.0286	0.596	0.991	0.617	13.5	42.6	46.3	12.5	0.495	0.813	−1.612
100	19.2	0.114	0.740	0.975	0.682	18.7	62.1	61.0	6.22	0.926	3.364	−1.509
150	11.3	0.0642	0	0.913	0.579	50.0	124.5	88.0	5.94	1.47	1.058	−1.394
200	10.3	0.0632	0	0.906	0.497	50.0	29.0	30.0	8.94	1.67	1.990	−1.101
300	9.17	0.0757	−2	0.865	−2		53.0		6.67	0.973	0.444	−0.907
500	6.89	0.419	−2	−2	−2				0.	8.60		
800	6.59	1.37	−2	−2	−2				0.	33.6		
1000	4.32	−1.68	−2	−2	−2				0.	30.4		
2000	2.44	−1.43	−2	−2	−2				0.	15.9		
3000	1.37	−1.03	−2	−2	−2				0.	4.01		

was to use experimental electron beam data and (or) theory, when the use of theoretical results was reasonable. We discuss below the elastic cross section and than the inelastic cross sections.

A. Elastic scattering

For elastic collisions by high-energy electrons it is conventional to employ the screened Rutherford cross section expressed as [19]

$$\sigma_R(E)=\sigma_0\frac{51.8\pi Z^2}{E^2\gamma(1+\gamma)}, \tag{1}$$

where Z is the atomic number of the substance (for argon $Z=18$), $\sigma_0=1\ \text{Å}^2$, and

$$\gamma=\gamma_s\frac{1.70\times10^{-5}Z^{2/3}}{\tau(\tau+2)}, \tag{2}$$

where $\tau=E/mc^2$ is the kinetic energy in units of the electron rest mass. Instead of evaluation of the screening parameter γ_s from Moliere theory [19], we take it equal to 1. Such a choice provides an agreement with experimental high-energy elastic cross section data. In the energy range of interest ($E\leqslant 10$ keV), $\tau\ll 2$, $\gamma=(29.8\ \text{eV})/E$, and, consequently, $\sigma_R=[(1800\ \text{eV})/E]\ \sigma_0$.

For elastic collisions of slower electrons the problem is more complicated and the theoretical methods have not been fully developed. In constructing elastic cross sections for any incident energy we piece together available experimental data at low E, and results applicable at higher E. We use the following formula for the elastic cross section:

$$\sigma_e=T\sigma_0\left[\frac{1}{1/E(1+u_1/E)(u_2^2+E^2)}+f\frac{g_1^2}{[(E-e')^2+g_1^2][1+(g_2/E)^2]}\right], \tag{3}$$

where $T=1800$ eV, and parameters u_1,u_2,f,g_1,g_2,e' are obtained from fitting of Eq. (3) to various empirical and theoretical determinations [20–29]. These parameters are given in Table II. The presented form decreases as $1/E$ for the high-energy limit [similar to the Rutherford cross section given by Eq. (1)] and contains the second term that describes the cross section maximum about 14 eV. This form is shown in Fig. 1.

TABLE II. Parameters used in Eq. (3).

Parameter	Value	Parameter	Value
u_1	372.888 eV	g_1	11.483 eV
u_2	2.101 eV	g_2	6.329 eV
f	0.013	e'	13.441 eV

The elastic collisions are very important in the scattering of electrons by atoms. Therefore, very accurate differential cross sections for the elastic scattering of electrons are needed in order to account for the behavior of electrons in gaseous media. In this study the elastic scattering in Ar was treated using the following phenomenological extension of the screened Rutherford formula:

$$\sigma_a(E,\theta)=\frac{1}{[1+2\gamma-\cos(\theta)]^2(1+\{(h_1+2)/[\cos(\theta)+2]\}^{d_1})}+B_1\frac{s^2/[s^2+(\theta+\theta')^2]}{(1+\{(h_2+2)/[\cos(\theta+\theta')+2]\}^{d_2})}+B_2\frac{1}{[1+2\mu-\cos(\theta)]^2\left(1+\left[\frac{h_3+2}{-\cos(\theta)+2}\right]^{d_3}\right)} \tag{4}$$

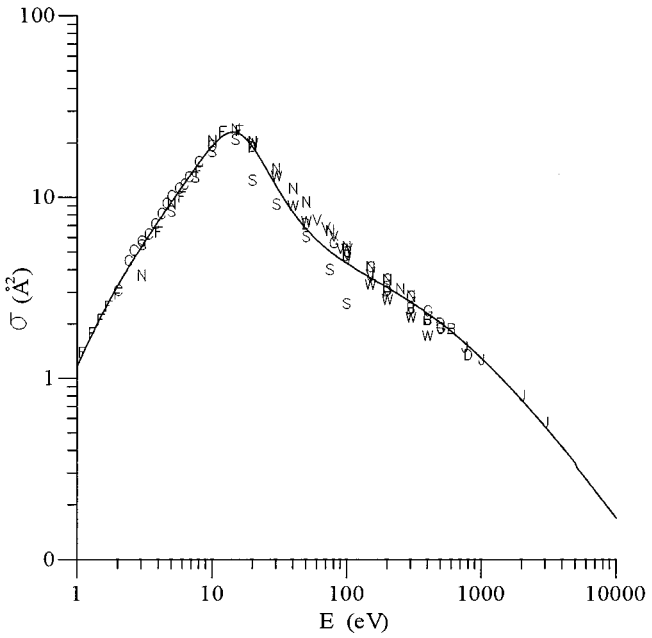

FIG. 1. Total elastic cross section. *B*: Bromberg [20]; *W*: Williams and Willis [21]; *G*: Gupta and Rees [22]; *D*: DuBois and Rudd [23]; *J*: Jansen *et al.* [24]; *V*: Vuskovic and Kurepa [25]; *C*: Charlton *et al.* [26]; *S*: Srivastava *et al.* [27]; *F*: Ferch *et al.* [28]; *N*: Nahar and Wadehra [29]. Line: Eq. (3).

where parameters $\gamma,\mu,h_1,h_2,h_3,d_1,d_2,d_3,B_1,B_2,s,\theta'$, presented in Table I, were found from fitting Eq. (4) to various experimental and theoretical determinations. [20–23,25,27,30,31]. The fitting for any incident energy was obtained using the spline interpolative technique [32]. Above 3 keV, the parameter γ was found by extrapolation of empirically determined dependence (shown in Table I) to provide agreement for energies above 50 keV with Eq. (2). The presented form transforms into the usual Rutherford cross section for a high-energy limit and contains two other terms (the second and third terms), which describe the medium-angle shape and backscatter enhancements. The comparison between various experimental and theoretical angular elastic cross sections, normalized for shape fitting only, and Eq. 4 at several selected energies is shown in Fig. 2.

B. Electronic excitation

In the case of excitation cross section, various analytic forms have been proposed to achieve asymptotic agreement with the results of the Born-Bethe approximation. In the nonrelativistic case a suitable form that is flexible for fitting data in the range from a high energy to the threshold energy is the following [18]:

$$\sigma_{\text{in}}(E)=q\frac{f_0}{W_j E}[1-(W_j/E)^{\alpha}]^{\beta}\Phi_j, \tag{5}$$

where $\Phi_j=\ln[4c_jE/W_j+e]$ is a ratio for allowed excitation, and $\Phi_j=[E/W_j]^{1-\Omega}$ is the ratio for the forbidden one, $q=6.513\ 10^{-14}\text{eV}^2\ \text{cm}^2$. The set of the most important electronic states of Ar was chosen using the analysis of Peterson and Allen [33] and Eggarter [34]. Table III presents a summary of information for several individual levels and groups of levels. The parameters for allowed transitions $4s_{3/2}$, $4s'_{1/2}$, $3d_{3/2}$, $3d'_{3/2}$, and for a composed forbidden state, were found from fitting Eq. (5) to the experimental data of Chutjian and Cartwright [14]. The value W for each state is the same as its threshold energy. For a composed allowed state we take a modified cross section from Eggarter [34]. It was changed so that our total inelastic cross section conforms with results from Heer *et al.* [35] at high energies (Fig. 3). For comparison we present in this figure the total inelastic cross section composed from partial cross sections of Peterson and Allen [33].

The ionization cross section data have been summarized recently in [36,37]. To reduce the cost of the Monte Carlo calculations in the present work the M-shell ionization (with threshold $I_m=15.76$ eV), the L -shell ionization (with threshold $I_m=250$ eV), and the K-shell ionization (with threshold $I_m=3.2$ keV) were not considered separately. We assume only one threshold at 15.76 eV. We chose the analytic formula for differential ionization cross section given by Green [1]:

$$S(E,e_s)=\frac{(K/E)\ln(E/J)\Gamma(E)^2}{\Gamma(E)^2+(e_s-e_s^0)^2}, \tag{6}$$

where e_s is the secondary electron energy, $\Gamma(E)=\Gamma_s E/(E+J), e_s^0=T_s-T_A/(E+T_B)$. But we modified the parameters K, J, Γ_s, T_s, T_A, T_B given in [1] in order to approximate both the experimental differential ionization cross sections obtained by Vroom *et al.* [38] and experimental total ionization cross sections from Heer *et al.* [35], Krishnakumar and Srivastava [39], Straub *et al.* [40]. The values of the parameters are presented in Table IV. Comparison of the total ionization cross section, which was obtained from integrating Eq. (6) over e_s, with experimental data from Heer *et al.* [35], Krishnakumar and Srivastava [39], and Straub *et al.* [40] is given in Fig. 4.

Figure 3 shows an agreement between the absorption cross section from Heer *et al.* [35] and the absorption cross section obtained as a sum of the ionization cross section and all electronically inelastic cross sections used in the present work. As a final test to the set of cross sections assembled, we compare in Fig. 5 the total cross section, which is a sum of the absorption and the elastic cross sections with results from various experimental and theoretical works [26,28–30,41,42].

III. CALCULATING PROCEDURE

With the updated set of cross sections we have carried out Monte Carlo computations for 0.1–10.0 keV incident electrons. Monoenergetic electrons were incident along the Z axis into the infinite homogeneous medium of gaseous argon. The computer program follows the electrons through a series of collisions. The details of the technique have been described in [17,43]. The incident electrons were followed down to the first excitation potential of argon. The number of primary particles at various incident energies was chosen such that the total number of ionization events is of the same order.

In this study the results of the electron distribution calculations were expressed in terms of electron flux determined

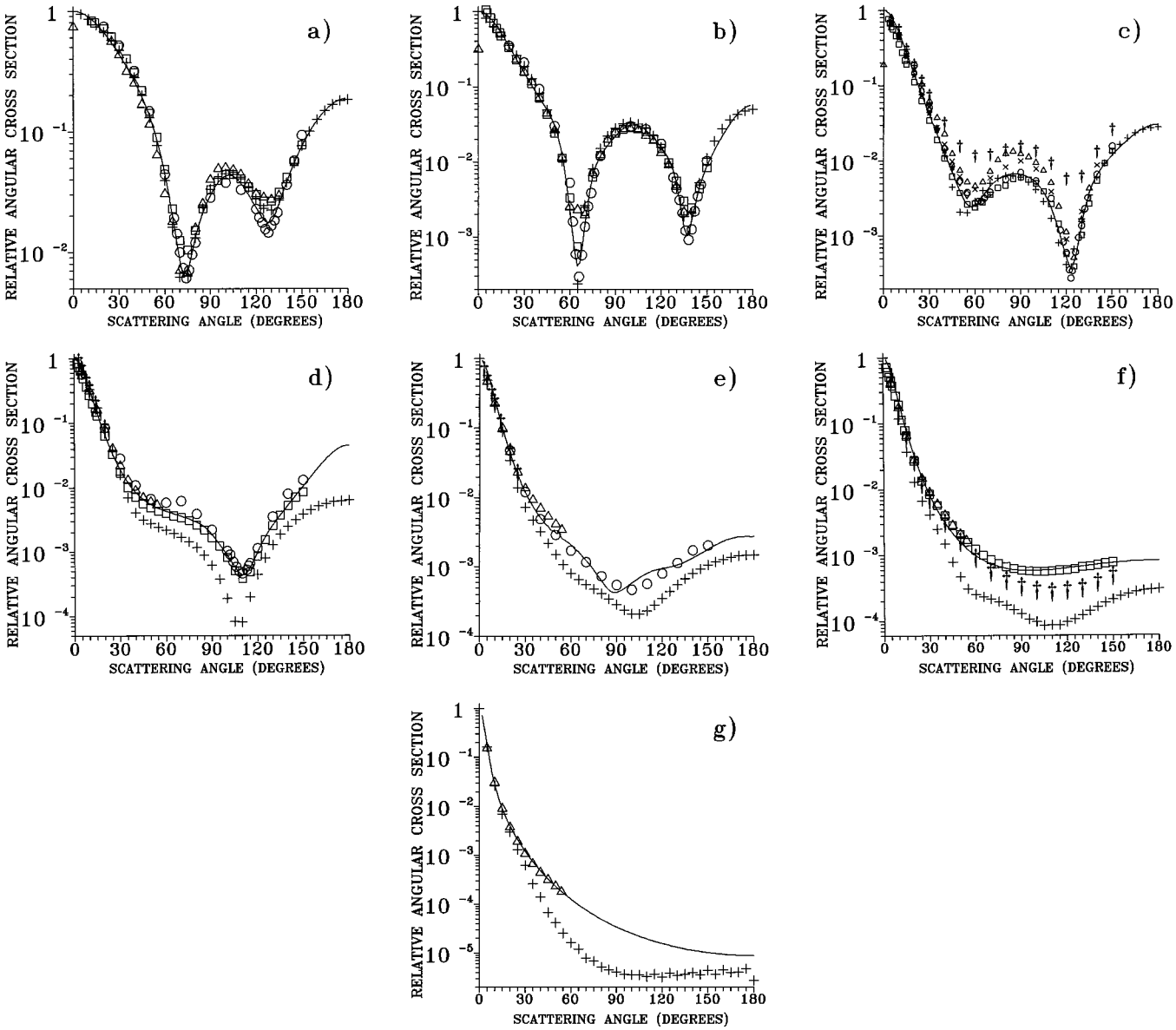

FIG. 2. Comparison of electron impact elastic differential cross sections from various authors at selected energies with Eq. (4) (solid line): (a) 20 eV; ○: Williams and Willis [21]; □: DuBois and Rudd [23]; △: Srivastava *et al.* [27]; +: Jain *et al.* [30]. (b) 50 eV, ○: Williams and Willis [21]; □: DuBois and Rudd [23]; △: Srivastava *et al.* [27]; +: Jain *et al.* [30]; (c) 100 eV; ○: Williams and Willis [21]; □: DuBois and Rudd [23]; △: Srivastava *et al.* [27]; +: Jain *et al.* [30]; ⋆: Vuskovic and Kurepa [25]; ◇: Jansen *et al.* [24]; ×: Gupta and Rees [22]; †: Webb [31]; (d) 200 eV; ○: Williams and Willis [21]; □: DuBois and Rudd [23]; △: Jansen *et al.* [24]; +: Jain *et al.* [30]; †: Bromberg [20]; (e) 400 eV; ○: Williams and Willis [21]; △: Jansen *et al.* [24]; +: Jain *et al.* [30]; †: Bromberg [20]; (f) 800 eV; △: Jansen *et al.* [24]; +: Jain *et al.* [30]; †: Webb [31]; □: DuBois and Rudd [23]; (g) 3 keV; △: Jansen *et al.* [24]; +: Jain *et al.* [30].

by multiplication of the distribution function and velocity. The electron flux was calculated with the following equation (primary electrons were incident along the Z axis):

$$\Phi(z,E)=\frac{(\Sigma_j[\nu_t(\vec{r}_j,E_j)/\sigma_t(E_j)])}{\Delta E\Delta z}. \tag{7}$$

Here $\nu_t(\vec{r}_j,E_j)=n_g\sigma_t(E_j(\vec{r}_j))v_j(\vec{r}_j)$ is the total collision frequency in position $\vec{r}_j$, v_j is the speed of the jth electron with energy E_j, and σ_t is the total cross section. The summation in Eq. (7) was implicated over all electrons existing in the spatial interval Δz centered at z, and, also, in the energy interval ΔE centered at E.

TABLE III. Parameters for argon excitation cross sections.

State	W_j	f_0	α	β	c_j	Ω
$4s_{3/2}$	11.6	0.051	0.288	0.807	0.212	
$4s'_{1/2}$	11.8	0.102	0.430	1.274	2.987	
$3d_{3/2}$	14.1	0.077	0.261	1.212	0.504	
$3d'_{3/2}$	14.3	0.131	0.216	1.395	0.604	
Composite						
Allowed	15.0	0.441	1.228	4.087	0.757	
Composite						
Forbidden	13.0	0.450	5.925	9.432		1.620

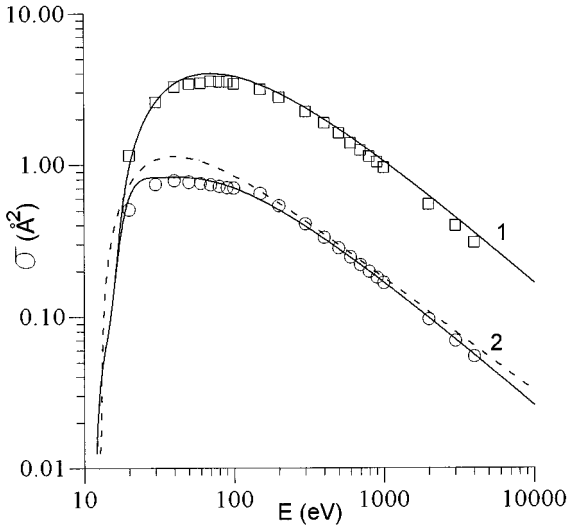

FIG. 3. Plot of absorption (1) and inelastic (2) cross sections: Heer *et al.* [35] (points), Peterson and Allen [33] (dashed line), and present results (solid lines).

IV. ENERGY ELECTRON DISTRIBUTION

In an attempt to test the validity of our approach the mean energies expended for production of various excited states of Ar were calculated by the formula $U_j = E_p / J$, where J is the number of excitations to state j, and E_p is incident energy. The mean energies for the five excited states and the ionization are shown in the sixth column of Table V, and compared with those obtained from results of Peterson and Allen [33], Keto [10], and Kimura and Inokuti [44]. In our calculations of the mean energy for ionization we applied the set of cross sections given in Sec. II, and the resulted energy was close to 27.1 and 26.81 eV obtained by Green *et al.* [9] and Kimura *et al.* [12], correspondingly. It is notably less than values from Peterson and Allen [33] and Keto [10]. Several reasons have been investigated. First we take the differential ionization cross section as the M-shell differential ionization cross section from Peterson and Allen [33] while keeping the set of inelastic cross sections presented in Sec. II. We found that this change slightly reduces the mean energy for the ionization, as one may expect, because the presented ionization cross section is smaller than that from Peterson and Allen for low energies (Fig. 4). Then, we completely replaced the set of cross sections summarized in this paper by that from Peterson and Allen [33]. The results obtained are given in the seventh column of Table V. Since the cross sections employed in the present calculations were identical to those from Peterson and Allen [33] and Keto [10], we attribute the difference between our results and those of Peterson and Allen [33] and Keto [10] to different calculating procedures.

TABLE IV. Parameters for argon differential ionization cross section.

Parameter	Value	Parameter	Value
K	13.947 Å^2 eV	T_s	2.294 eV
J	15.760 eV	T_A	68.820 eV^2
Γ_s	8.602 eV	T_B	51.505 eV

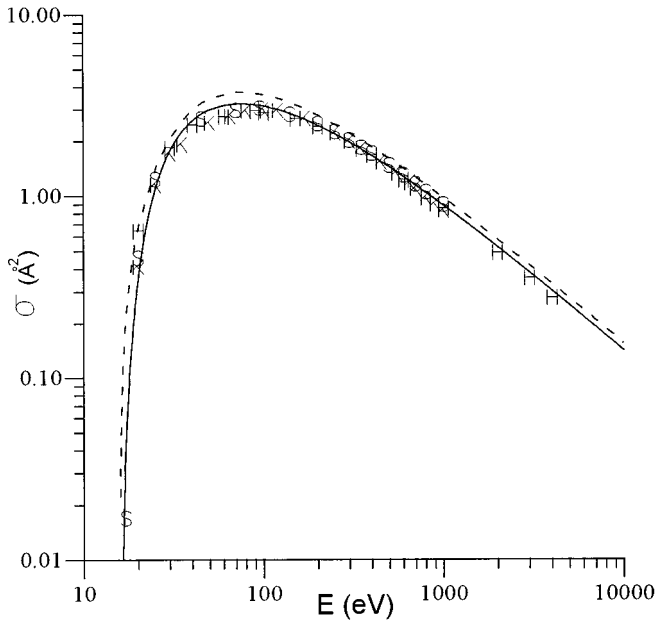

FIG. 4. Plot of total ionization cross sections. H: Heer *et al.* [35]; K: Krishnakumar and Srivastava [39]; S: Straub *et al.* [40]; dashed line: Peterson and Allen [33]; solid line: present results.

The mean energy required for production of the ion-electron pair of 26.06 (for 10 keV incident electron) is in a good agreement with the reported experimental values near 26.4 eV [45]. It should be pointed out that the mean energy obtained in this study for production of an ion-electron pair is close to 25.4 eV, which was obtained by Bretagne *et al.* [46] for calculation of the balance of the energy deposited for a narrow energy dispersion of primary electrons.

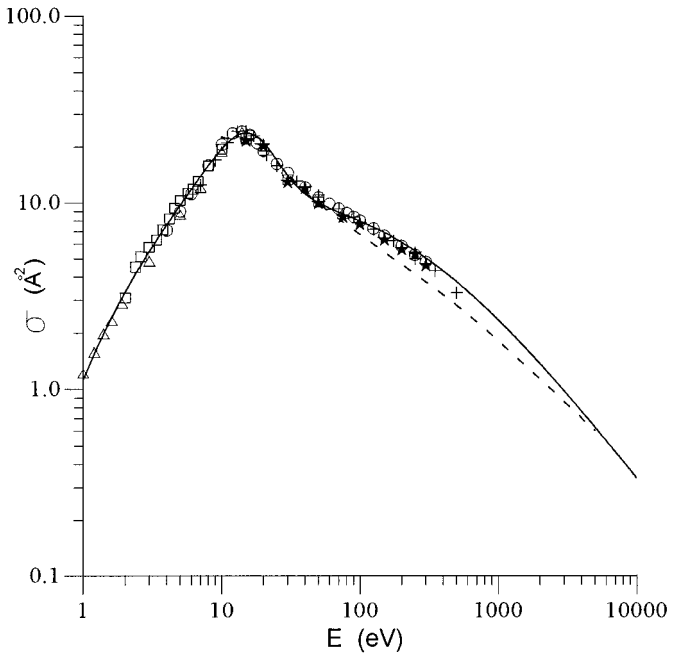

FIG. 5. Comparison of present total cross section (solid line) with various empirical and theoretical determinations. □: Charlton *et al.* [26]; △: Ferch *et al.* [28]; ⋆: Nahar and Wadehra [29]; dashed line: Jain *et al.* [30]; +: Nishimura and Yano [41]; ○: Nickel *et al.* [42].

TABLE V. Mean energy expended per an inelastic excitation by electrons in argon. I and II: results obtained using corresponding set of cross sections presented in Sec. II and that from Peterson and Allen [33].

State	W_j	U_j (Keto)	U_j (Peterson and Allen)	U_j	U_j^I (This work)	U_j^{II} (This work)
$4s_{3/2}$	11.6	974.79	773.3		305.40	510.20
$4s'_{1/2}$	11.8	261.06	268.2	230[a]	200.82	190.75
$3d_{3/2}$	14.1	1101.56	1175.		1701.58	880.05
$3d'_{3/2}$	14.3	893.75	752.6		1538.56	734.54
Forbidden	13.0	242.54	236.4		280.51	198.41
Ion	15.76	33.53	30.3	26.81[b]	26.28	27.21

[a]Kimura and Inokuti [44].
[b]Kimura *et al.*[12].

Having established a reasonable agreement between the present computations and earlier works, we used the Monte Carlo method to compute the electron flux. The electron flux density, which is electron flux normalized to the gas density and total ionization rate, is shown in Fig. 6 for four incident energies. In a qualitative sense, these four flux densities have a similar energy dependence. Therefore, we restrict the discussion of energy dependence of flux density to the case of 1.0 keV incident electrons. At low energies, this flux density goes down with a rise in energy; this is due to an increase in the ratio of inelastic collision number to elastic collision number with energy. The flux density has a minimum at about 200 eV. Then it starts to increase gradually. The flux density increases rapidly near the incident energy. Electron flux or the electron degradation spectrum in Ar was extensively studied by Kimura *et al.* [13]. Basically, the results presented in Fig. 6 are in agreement with those from Kimura *et al.* [13]. But, we do not observe in our results a sharp spike at moderate energies because of the Auger effect; and there is no slight shoulder near the threshold energy, because of the contribution from the excitation of metastable states. These are a result of using more simple models for simulation of ionization and excitation of metastable states than Kimura *et al.* [13].

Figure 6 shows that the low-energy electron distribution ($E \leqslant 60$ eV) is practically independent of incident electron energy. The reason for this is as follows. The low-energy electron distribution is basically formed by secondary electrons of different generations. By secondary electrons we mean electrons produced by ionization. There are two important factors determining the formation of the secondary electron distribution: (i) any secondary electron produced, on the average, had a small energy close to the electron excitation of the atom; (ii) the energy of a secondary electron was practically independent of the incident energy. Taking into account the peculiarity of the low-energy electron distribution, the numerical electron flux density can be approximately represented analytically by

$$\Phi_a(E,E_p)=\sum_{k=1}^{3} \Xi_k \overline{E}^{-\lambda_k}+\Theta \overline{E}^{\nu}/E_p, \tag{8}$$

where $\overline{E}=E/(1\ \text{keV})$ and the values of parameters used in Eq. (8) are presented in Table VI. Equation (8) represents the flux data fairly well for 0.5–100.0 keV incident electrons (Fig. 6). Taking into account that the convolution integral of the electron flux density with ionization cross section is equal to 1 [47], the efficiency for production of the jth state can be calculated using the formula

$$\epsilon_j^q(E_p)=(W_j/U_i^q)\int_0^{E_p}\Phi_a(E,E_p)\sigma_j(E)dE, \tag{9}$$

where $U_i^q = 26$ eV.

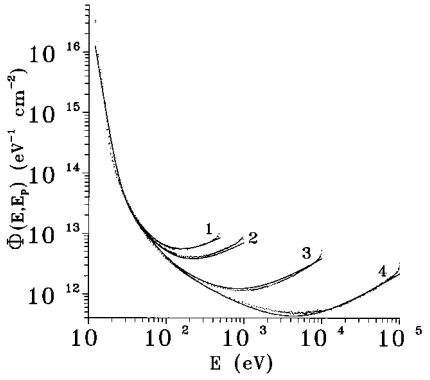

FIG. 6. Electron flux density. 1: E_p = 0.5 keV; 2: E_p = 1.0 keV; 3: E_p = 10.0 keV; 4: E_p = 100.0 keV. The Monte Carlo calculations are shown by the points and the analytic fit using Eq. (8) is represented by the solid lines.

V. RANGES AND SPATIAL DEPENDENCIES OF EFFICIENCIES

One of the important characteristics of electron-beam-generated plasma is a range, i.e., a path length that electrons pass as their energy decreases from E_p to the minimum energy. The longitudinal energy deposition plots were computed and used to calculate the practical ranges (R_0) for electrons. These ranges, presented in Table VII, were found

TABLE VI. Parameters used in Eq. (8).

Parameter	Value	Parameter	Value
Ξ_1	2.05	λ_1	8.264
Ξ_2	9.79×10^{9}	λ_2	2.198
Ξ_3	5.57×10^{11}	λ_3	0.601
Θ	6.15×10^{12}	ν	0.749

TABLE VII. Range of data (in 10^{-6} g/cm^2) at selected incident energies (in keV).

E_p	R_0
0.1	0.68
0.5	3.82
1.0	9.60
2.0	27.07
2.5	37.84
3.0	54.20
5.0	131.68
10.0	435.06

by extrapolation of the linear portion of the energy deposition curves to the Z axis.

The energy deposition plots for 0.5–10.0 keV incident electrons is shown in Fig. 7. The results presented in the figure are normalized such that the integral of the area under each curve equals 1. The abscissa in Fig. 7 is the reduced depth (related to the range determined in this study). The energy deposition behind the injection point is due to backscattered electrons, while the energy deposition jump at the injection point is due to the contribution from the collimated beam. Curves computed for incident electrons of 0.5, 1.0, and 2.0 keV fit closely. The peak of curves shifts to a deeper depth for higher energies. For this set of curves the shape remains the same.

The most complete information about interaction of electron beam with gas, in our opinion, contains in the electron flux. The electron flux density $\Phi(E,z)$ (for 1.0 keV incident electrons) as a function of distance to the point of injection is given in Fig. 8. [We denote the results of the flux density calculations averaged over the space as $\Phi^{(\mathrm{avr})}(E)$.] $\Phi(E,z)|_{z/R_0=0.028}$ is rather similar to $\Phi^{(\mathrm{avr})}(E)$, but it lies below than $\Phi^{(\mathrm{avr})}(E)$ at moderate energies and exceeds $\Phi^{(\mathrm{avr})}(E)$ at the incident energy. $\Phi(E,z)|_{z/R_0=0.235}$ closely follows $\Phi(E,z)|_{z/R_0=0.028}$ below 120 eV. Then $\Phi(E,z)|_{z/R_0=0.235}$ starts increasing gradually with increase in energy. Near the incident energy $\Phi(E,z)|_{z/R_0=0.235}$ decreases rapidly, while $\Phi(E,z)|_{z/R_0=0.028}$ increases. Finally, we compare flux density calculated at $z/R_0 = 1.064$ with $\Phi^{(\mathrm{avr})}(E)$. Below 30 eV, these two quantities are practically identical. $\Phi(E,z)|_{z/R_0=1.064}$ is invariant with increasing energy at $100<E<400$ eV. Above 400 eV, $\Phi(E,z)|_{z/R_0=1.064}$ and $\Phi^{(\mathrm{avr})}(E)$ show quite distinctive features. Specifically, $\Phi(E,z)$ sharply decreases as energy increases, while $\Phi^{(\mathrm{avr})}(E)$ gradually increases. To put it another way, Fig. 8 shows that with distance from the point of injection the energy spectrum of flux density becomes exhausted with high-energy electrons. This is because of the energy degradation and scattering of the electron beam. As a contrast to the high-energy range, various curves, given in Fig. 8, are practically identical in the low-energy range. A similar result was obtained by Jackman and Green [16] for molecular nitrogen. The reason for this is the peculiarities of the secondary electron distribution formation, which was discussed above.

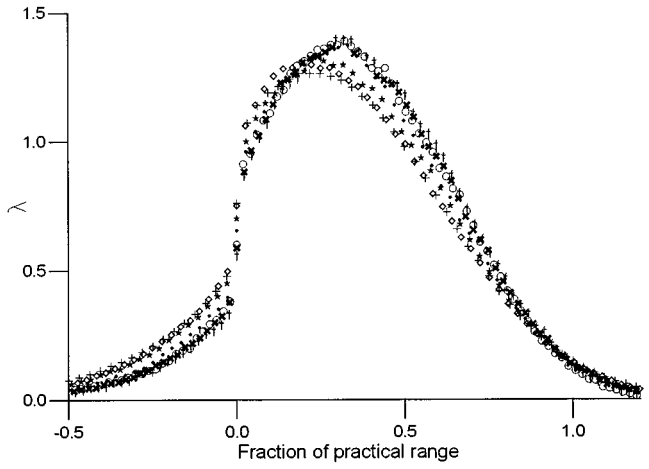

FIG. 7. Energy deposition (λ). +: E_p=0.5 keV; ◇: E_p=1.0 keV; ⋆: E_p=2.0 keV; ●: E_p=2.5 keV; ×: E_p=3.0 keV; ○: E_p =5.0 keV, †: E_p=10.0 keV.

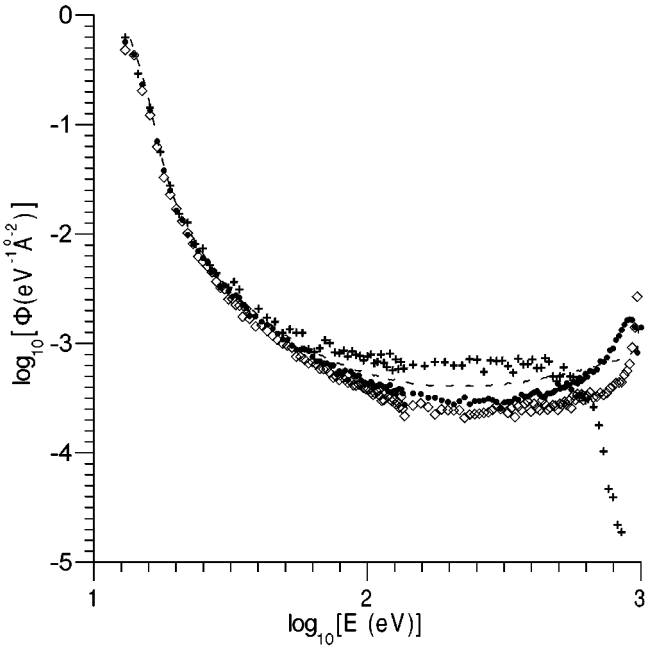

FIG. 8. Electron flux density as a function of distance to the injection point. ◇: z/R_0=0.028; ●: z/R_0=0.235; +: z/R_0=1.064. Dashed line: $\Phi^{(\mathrm{avr})}(E)$. E_p=1.0 keV.

For the purposes of many applications, the analytical formula for the electron flux may be approximately expressed by multiplication of the space- and energy-dependent terms. The reason for this approximation is that the low-energy electron distribution is practically independent of the distance to the point of the injection. If the electron flux is known, it is possible to calculate the efficiency for production of any electron state. Figure 9 shows the ratio of the efficiency for the production of the composite forbidden state to that for ionization as a function of distance to the injection point for incident electrons of 0.5 keV (+), 1.0 keV (◇), and 10.0 keV (●). Solid lines show Monte Carlo calculation results being averaged over the space. Results manifest that the ratio slightly increases with a distance to the point of injection for incident electrons of 0.5 and 1.0 keV, and it is almost independent of distance for 10.0 keV electrons. Taking into consideration that the energy dependence for the

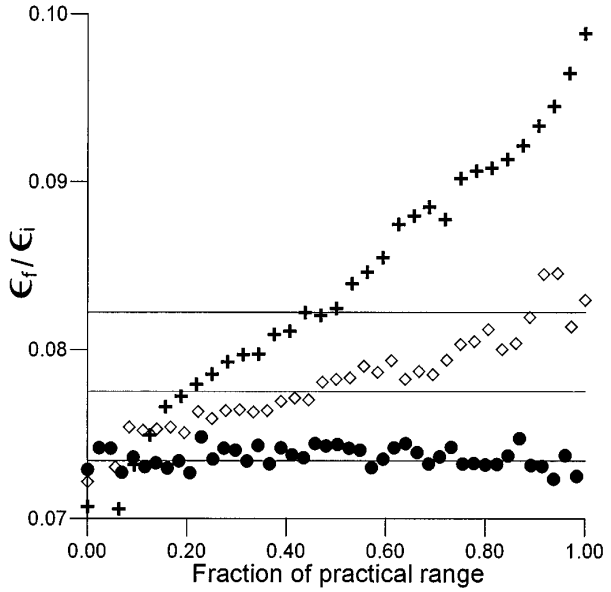

FIG. 9. Ratio of the efficiency (ϵ_f) for production of composite forbidden state to efficiency (ϵ_i) for ionization.

ionization cross section and that for the cross section of excitation of composite forbidden state are clearly different, it should be expected that the tendency similar to that displayed by Fig. 9 also exists for other excitation states of argon.

The efficiency for production of any state may be expressed as

$$\epsilon_j^A(z,E_p)=\epsilon_j^a(E_p)\Psi(z), \tag{10}$$

where ϵ_j^a was found from Eq. (9) and the spatial term was determined by the expression [48]

$$\Psi(z)=(a_0)^{-1}\exp\{a_1 z-a_2(z+a_3)^2\}.$$

The distance along the Z axis was expressed in $R_a=1.27+7.90\,E_p^{1.740}$, and the values of other parameters are given in Table VIII.

The curves of efficiencies for production of ionization and the composite forbidden state, and also of the combined efficiency obtained as a sum of the efficiencies for each electronic state calculated by the Monte Carlo method are plotted in Fig. 10. These curves are compared with the analytical function [Eq. (10)]. The agreement confirms the adequacy of proposed analytical function.

Figure 10 shows that the shape of any efficiency is practically independent of the electron state and it is invariant with the increasing in the incident energy; these results are in agreement with those shown in Fig. 9. This is due to the fact

TABLE VIII. Parameters used in Eq. (10).

Parameter	$E_p \leqslant 2$ keV	2 keV$<E_p<$3 keV	$E_p \geqslant 3$ keV
a_0	0.96	$0.74+0.15E_p$	1.19
a_1	2.17	$-0.61+1.39E_p$	3.56
a_2	4.06	$2.04+1.01E_p$	5.07
a_3	0.0043	$-0.05+0.027E_p$	0.031

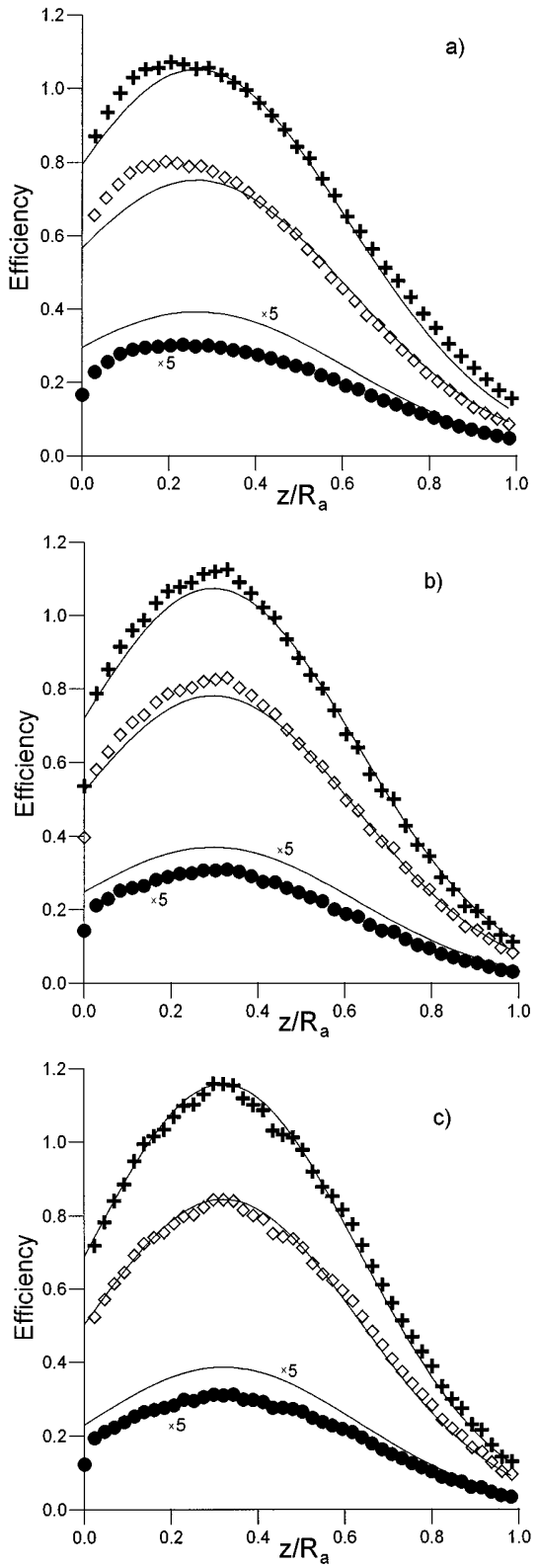

FIG. 10. Spatial dependencies of the efficiencies for production of composite forbidden state (●), ionization (◇), and combined efficiencies (+); (a) E_p=1.0 keV, (b) E_p=2.5 keV, (c) E_p=10.0 keV.

that the low-energy electron distribution (which contributes predominantly to the excitation of all electron states) is practically independent of distance from the injection point and incident energy. Near the injection point, the efficiencies in-

TABLE IX. Parameters used in Eq. (11).

Parameter	Value
Λ	0.027
D_0	−49.83
D_1	73.30
η	0.418
ξ	1.638

crease with distance. The reason for that is as follows. The average energy of the beam reduces with distance from the injection point. Consequently, the efficiency for production of any electron state increases; this is because the excitation cross section of any electron state increases with an energy decrease in the energy range above 100 eV. The efficiencies have a maximum approximately at $z/R_a=0.2$ for 1.0 keV incident electrons, and at $z/R_a=0.3$ for 2.5 keV and 10.0 keV incident electrons. Then, an increase in distance lowers the efficiencies; this is because the excitation cross section of any electron states decreases with an energy decrease at low energies.

VI. DISCUSSION

To describe the range of data in solids, Feldman [49] developed an analytical expression for a stopping power that is a phenomenological extension of Born-Bethe's relation [50]. In this study, to determine the range of data in gases, we use the following equation:

$$R=\Lambda(A_0/Z^{\eta})+\sum_{k=0}^{1} D_k(A_0/Z^n)^k(E_p)^{\xi}, \qquad (11)$$

where A_0 is the atomic or molecular weight of the material, Z is the atomic number or the number of electrons per molecule in the case compounds, and $n=1.60/[1+0.063\ln(Z)]$. Parameters are presented in Table IX. Equation (11) indicates a stronger dependence on the atomic number than had been previously suspected by Singhal and Green [51]. A comparison of various theoretical and experimental data with Eq. (11) for molecular hydrogen, atomic oxygen, molecular nitrogen, and argon is shown in Fig. 11. The practical range versus energy for atomic oxygen was obtained from the effective range versus energy function for atomic oxygen [51] corrected by a factor that is a ratio of practical [16] to effective [52] ranges calculated for nitrogen. This appears reasonable since the cross sections in nitrogen and oxygen are rather similar.

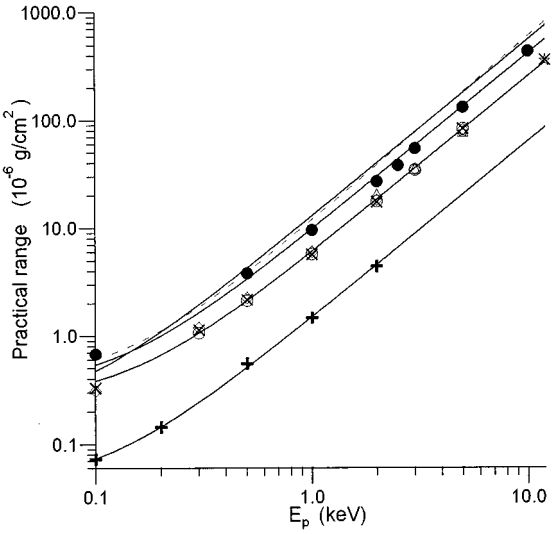

FIG. 11. Practical range versus incident energy. Molecular hydrogen: Heaps and Green [53] (+); atomic oxygen: Singhal and Green [51] (dashed line); molecular nitrogen: Grun [54] (⋆); Cohn and Caledonia [55] (△); Barrett and Hays [56] (○); Porter *et al.* [57] (×); Vasenkov [43] (◇); argon: present results (●). Lines: Eq. (11).

VII. CONCLUSIONS

In this study computations have been carried out by the Monte Carlo method for 0.1–10.0 keV incident electrons. Throughout the energy range the integral and differential cross sections employed in the model are in agreement with measurements. Our results on the electron-energy-degradation process are compared with previous data.

The energy- and space-dependent flux of electrons was calculated. The proposed analytical formula for the flux can be applied conveniently to the calculation of efficiency for production of any state at any spatial position along the beam axis.

The range versus energy expression [Eq. (11)] for various gaseous media was obtained and compared successfully with the range of data available from the current literature.

ACKNOWLEDGMENT

This work was supported by Grant No. 96-03-33924a of the Russian Foundation of Basic Researches.

[1] A. E. S. Green, Radiat. Res. **64**, 119 (1975).
[2] I. A. Krinberg, *Kinetics of Electrons in the Ionosphere of the Earth* (Nauka, Moscow, 1978).
[3] Z. Yu, C. A. Moore, and G. J. Collins, J. Vac. Sci. Technol. A **5**, 1759 (1987).
[4] Z. Yu, Z. Luo, T. Y. Sheng, H. Zarnani, C. Lin, and G. J. Collins, IEEE Trans. Plasma Sci. **18**, 753 (1990).
[5] S. Matsui, T. Ichihashi, and M. Mito, J. Vac. Sci. Technol. B **7**, 1182 (1989).
[6] R. G. Sharafutdinov, A. V. Skrynnikov, A. V. Parakhnevich, B. M. Ayupov, A. M. Badolian, O. V. Polyakov, M. R. Baklanov, K. P. Mogilnikov, and S. A. Biryukov, J. Appl. Phys. **79**, 7274 (1996).
[7] U. Kortshagen and H. Schluter, J. Phys. D **25**, 644 (1992).

[8] C. J. Elliot and A. E. Greene, J. Appl. Phys. **47**, 2946 (1976).
[9] A. E. S. Green, C. H. Jackman, and R. H. Garvey, J. Geophys. Res. **82**, 5104 (1977).
[10] J. W. Keto, J. Chem. Phys. **74**, 4445 (1981).
[11] K. Kowari, M. Kimura, and M. Inokuti, Phys. Rev. A **39**, 5545 (1989).
[12] M. Kimura, I. Krajcar-Bronic, M. A. Dillon, and M. Inokuti, Phys. Rev. A **45**, 7831 (1992).
[13] M. Kimura, M. Inokuti, and M. A. Dillon, in *Advances in Chemical Physics*, edited by I. Prigogine and S. A. Rice (Wiley, New York, 1993), Vol. 84, p. 193.
[14] A. Chutjian and D. C. Cartwright, Phys. Rev. A **23**, 2178 (1981).
[15] R. D. DuBois and M. E. Rudd, Phys. Rev. A **17**, 843 (1978).
[16] C. H. Jackman and A. E. S. Green, J. Geophys. Res. **84**, 2715 (1979).
[17] V. S. Malinovsky and A. V. Vasenkov, Phys. Rev. E **50**, 4969 (1994).
[18] H. S. Porter, C. H. Jackmann, and A. E. S. Green, J. Chem. Phys. **65**, 154 (1976).
[19] G. Moliere, Z. Naturforsch. A **3**, 78 (1948).
[20] J. P. Bromberg, J. Chem. Phys. **61**, 963 (1974).
[21] J. F. Williams and B. A. Willis, J. Phys. B **8**, 1670 (1975).
[22] S. C. Gupta and J. A. Rees, J. Phys. B **8**, 1267 (1975).
[23] R. D. DuBois and M. E. Rudd, J. Phys. B **9**, 2657 (1976).
[24] R. H. Jansen, F. J. de Heer, H. J. Luyken, B. van Winggerden, and H. J. Blaauw, J. Phys. B **9**, 185 (1976).
[25] L. Vuskovic and M. V. Kurepa, J. Phys. B **9**, 837 (1976).
[26] M. Charlton, T. C. Griffith, G. R. Heyland, and T. R. Twomey, J. Phys. B **13**, L.239 (1980).
[27] S. K. Srivastava, H. Tanaka, A. Chutjian, and S. Trajmar, Phys. Rev. A **23**, 2156 (1981).
[28] J. Ferch, B. Granitza, C. Masche, and W. Raith, J. Phys. B **18**, 967 (1985).
[29] S. N. Nahar and J. M. Wadehra, Phys. Rev. A **43**, 1275 (1991).
[30] A. Jain, B. Etemadi, and K. R. Karim, Phys. Scr. **41**, 321 (1990).
[31] G. M. Webb, Phys. Rev. **47**, 379 (1935).
[32] Carl de Boor, *A Practical Guide to Splines* (Springer-Verlag, New York, 1985).
[33] L. R. Peterson and J. E. Allen, J. Chem. Phys. **56**, 6068 (1972).
[34] E. Eggarter, J. Chem. Phys. **62**, 833 (1975).
[35] F. J. de Heer, R. H. J. Jansen, and W. van der Kaay, J. Phys. B **12**, 979 (1979).
[36] ICRUM, ''Secondary electron spectra from charged particle interactions'' (International Commission on Radiation Units and Measurements Report No. 55, 1996).
[37] IAEA, ''Atomic and molecular data for radiotherapy and radiation research,'' International Atomic Energy Agency, Report No. IAEA-TECDOC-799, 1995.
[38] D. A. Vroom, R. L. Palmer, and J. Wm. McGowan, J. Chem. Phys. **66**, 647 (1977).
[39] E. Krishnakumar and S. K. Srivastava, J. Phys. D **21**, 1055 (1988).
[40] H. S. Straub, P. Renault, B. G. Lindsay, K. A. Smith, and R. F. Stebbings, Phys. Rev. A **52**, 1115 (1995).
[41] H. Nishimura and K. Yano, J. Phys. Soc. Jpn. **57**, 1951 (1988).
[42] J. C. Nickel, K. Imre, D. F. Register, and S. Trajmar, J. Phys. B **18**, 125 (1985).
[43] A. V. Vasenkov, Ph.D. dissertation, Institute of Thermophysics, Novosibirsk, 1996.
[44] M. Kimura and M. Inokuti, J. Chem. Phys. **87**, 3875 (1987).
[45] Yu. I. Bychkov, Yu. D. Korolev, G. A. Mesyats, V. V. Osipov, V. V. Ryzhov, and V. F. Tarasenko, *Injection Gas Electronics* (Nauka, Novosibirsk, 1982).
[46] J. Bretagne, G. Delouga, J. Godart, and V. Puech, J. Phys. D **14**, 1225 (1981).
[47] V. P. Konovalov and E. E. Son, Zh. Teckh. Fiz. **50**, 300 (1980) [Sov. Phys. Tech. Phys. **25**, 178 (1980)].
[48] A. E. S. Green and R. P. Singhal, Geophys. Res. Lett. **6**, 625 (1979).
[49] C. Feldman, Phys. Rev. **117**, 455 (1960).
[50] F. Rohrlich and B. C. Carlson, Phys. Rev. **93**, 38 (1954).
[51] R. P. Singhal and A. E. S. Green, J. Geophys. Res. **86**, 4776 (1981).
[52] R. P. Singhal, C. H. Jackman, and A. E. S. Green, J. Geophys. Res. **85**, 1246 (1980).
[53] M. G. Heaps and A. E. S. Green, J. Appl. Phys. **45**, 3183 (1974).
[54] A. E. Grun, Z. Naturforsch. A **12**, 89 (1957).
[55] A. Cohn and G. Caledonia, J. Appl. Phys. **41**, 3767 (1970).
[56] J. L. Barrett and P. B. Hays, J. Chem. Phys. **64**, 743 (1976).
[57] H. S. Porter, F. Varosi, and H. G. Mayr, J. Geophys. Res. A **92**, 5933 (1987).